Nanotechnology

Fabrication of Metal–Semiconductor Nanowire Heterojunctions

Jinhua Zhan, Yoshio Bando, Junqing Hu, Zongwen Liu, Longwei Yin, and Dmitri Golberg*

One-dimensional nanostructures play an important role in nanotechnology for their use as building blocks in nanoscale circuits, and in optoelectronic, electrochemical, and electromechanical devices.[1] Nanotubes, nanobelts, nanorods, and semiconducting nanowires have been fabricated through a number of advanced nanolithographic techniques, thermal evaporation, and solution-based methods.[2] For the development of a wide selection of nanoscale building blocks for nanometer-sized electrical and optical lines with new properties, it is important that the potential barrier between adjacent constituents has the appropriate current–voltage characteristics. This can be realized by the creation of various heterostructures including p–n junctions, metal–oxide–semiconductor junctions, or metal–semiconductor contacts that allow reliable signal processing.[3] Diverse heterostructures assembled in either radial or axial directions within a single nanometer-scale building block have been fabricated.[4–9] These include the axial block-by-block groups III-V (GaAs/GaP, InAs/InP) and group IV (Si/Ge) semiconductor nanowires, epitaxial Si/Ge core–shell nanowire heterostructures, heterojunctions of carbon nanotubes and silicon nanowires, and NiSi/Si nanowire heterostructures.

Silicon has long been considered the prime material for information-technology electronics.[10] It has recently been found valuable for photonics as well.[11] Silicon nanowires are particularly important for the miniaturization of Si-integrated circuits (IC). Various approaches including vapor-liquid-solid (VLS) growth, solution-liquid-solid (SLS) growth, and oxide-assisted (OA) growth, have been used for the synthesis of Si nanowires.[12] Metallic nanowires that display novel magnetic or electrical properties have been extensively studied.[13–16]

Upon connection of a metallic nanowire to a semiconducting Si nanowire, a unique metal–semiconductor nanoscale contact can be prepared as a fundamental component of a novel miniaturized semiconductor device. The metal–semiconductor nanowire junctions are sheathed with insulating silicon oxide. Herein, we demonstrate the fabrication of In–Si end-to-end nanowire contacts and present a thorough analysis of their morphological and structural characteristics.

Thermal evaporation of an In/SiO powder mixture in an induction furnace results in the generation of a gray-colored product in the outlet of a graphite induction-heated cylinder. A powder XRD pattern (Figure 1) of the product initially

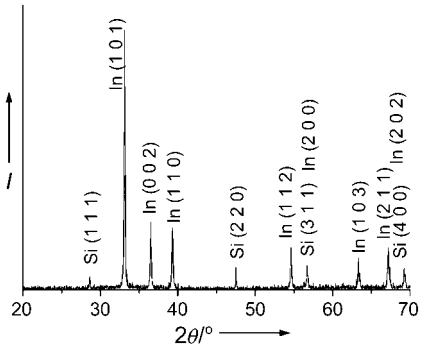

Figure 1. XRD pattern of the product of thermal evaporation of an In/SiO powder mixture in an induction furnace.

suggested the coexistence of diamond-cubic silicon (JCPDS file 27-1402) and tetragonal indium (JCPDS file 05-0642). Detailed structural and chemical analyses of the products were further carried out with TEM, high-resolution TEM (HRTEM), electron diffraction (ED), and energy-dispersive X-ray spectroscopy (EDS). Figure 2a shows a TEM micrograph of a typical nanowire junction. The nanostructure is composed of two distinct end-to-end segments. The bottom gray-contrast portion is several micrometers in length. The length of the upper black-contrast portion reaches dozens of micrometers (it is only partially shown in Figure 2a). The diameter of the 1D nanostructure is $\approx$200 nm. EDS spectra generated with an electron nanoprobe ($\approx$20 nm) were collected from three spots along the nanostructure: the upper tubelike segment, the black-contrast segment, and the gray-contrast segment as indicated by the corresponding circles in Figure 2a. The respective results are shown in Figure 2b–d. The tube is silicon oxide with a composition of 68.6% oxygen and 31.4% silicon. The dark-contrast branch is composed of indium; the gray-contrast branch is made of silicon. The O peaks in Figure 2c and d may originate from a Si oxide sheath on the In and Si nanowires, respectively, whereas the C and Cu signals come from a C-coated Cu TEM grid. EDS elemental mapping sheds additional light on the nanowire-junction chemistry. Figure 3a is a scanning transmission electron microscopy (STEM) image of an In–Si end-to-end nanowire heterojunction. This reveals a clear interface between the two domains. The respective In, Si, and O elemental maps are shown in Figures 3b–d. They demonstrate well-defined composition variations and the sharp interface between the In and Si segments. The uniform oxygen scattering originates from the amorphous silicon oxide that sheaths the entire nanowire. Notably, nearly all Si nanowires observed during extensive TEM studies were connected with In nanowires to display the In–Si heterojunction morphology.

[*] Dr. J. Zhan, Prof. Y. Bando, Dr. Z. Liu, Dr. L. Yin, Prof. D. Golberg
Advanced Materials Laboratory and Nanomaterials Laboratory
National Institute for Materials Science
Namiki 1-1, Tsukuba, Ibaraki 305-0044 (Japan)
Fax: (+81) 29-851-6280
E-mail: zhan.jinhua@nims.go.jp
Dr. J. Hu
International Center for Young Scientists (ICYS)
National Institute for Materials Science (NIMS)
Namiki 1-1, Tsukuba, Ibaraki 305-0044 (Japan)

Supporting information for this article is available on the WWW under http://www.angewandte.org or from the author.

  DOI: 10.1002/ange.200462813

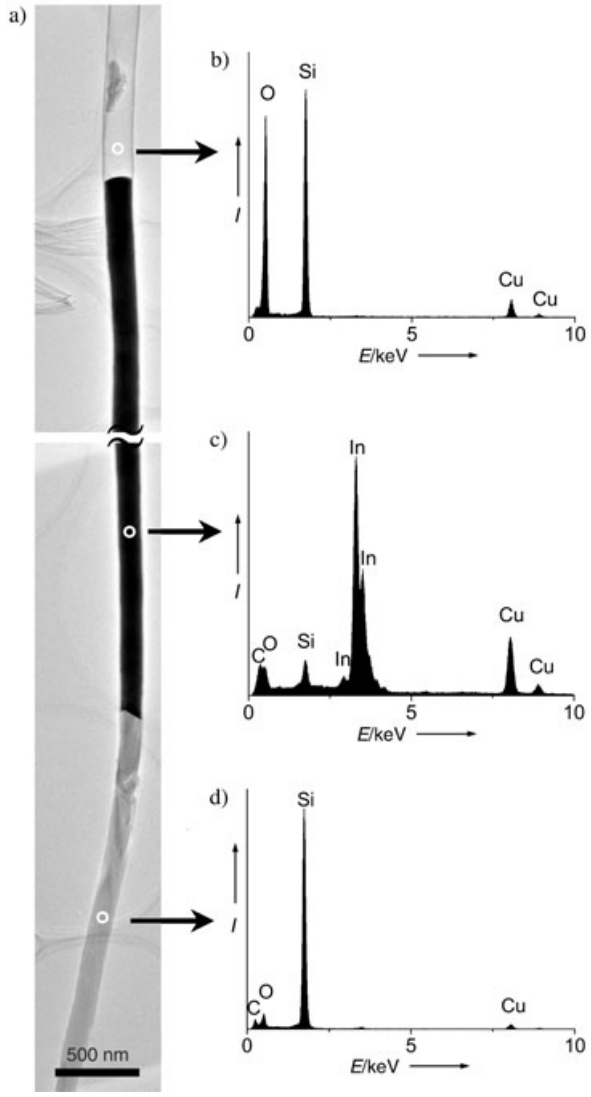

Figure 2. a) TEM image of a typical In–Si nanowire heterojunction; b)–d) respective EDS spectra taken from the regions indicated with the white circles on the nanowire image of part a).

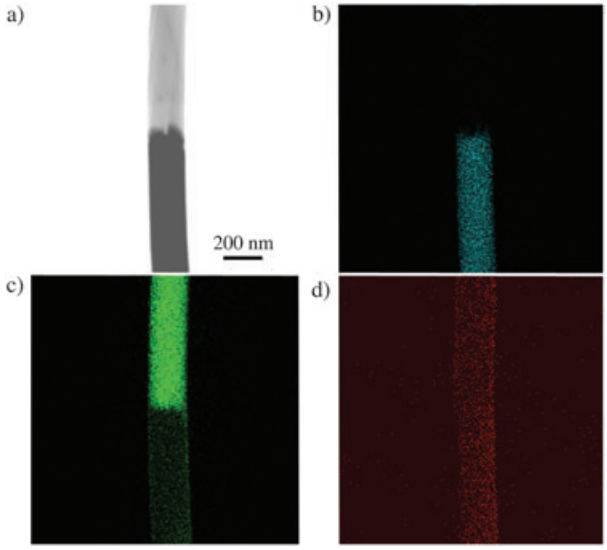

Figure 3. a) STEM image depicting Si (light) and In (dark) domains within an In–Si nanowire junction; b) In; c) Si; and d) O elemental maps demonstrating the elemental-spatial distribution.

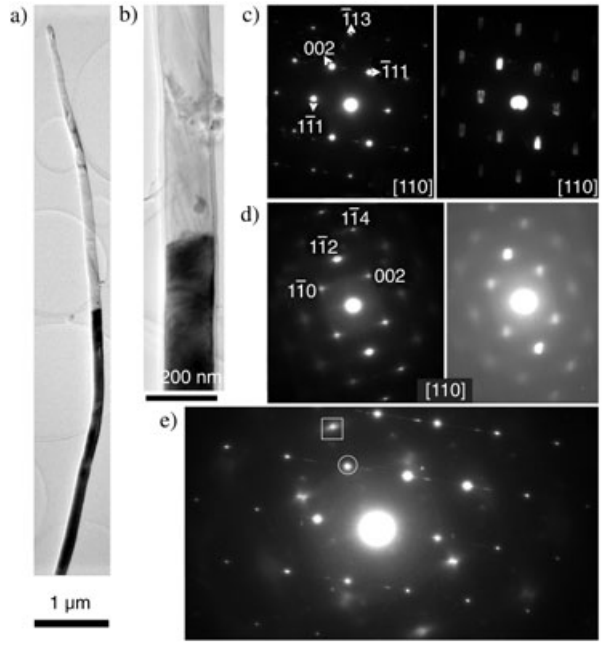

Figure 4. a) TEM image of a single In–Si nanowire junction; b) magnified TEM image that shows the In–Si nanowire junction is uniformly sheathed with silica; c)–e) respective SAED patterns taken from the selected Si, In, and In–Si boundary regions.

Detailed TEM investigations provided further insight into the heterojunction microstructure. Figure 4a depicts a representative In–Si nanowire heterojunction. Figure 4b shows its magnified view. It is apparent that the entire nanowire junction is uniformly coated with an 8-nm-thick silicon oxide sheath. Selected area electron diffractions (SAED) were taken from a Si nanowire segment (light contrast), an In nanowire segment (dark contrast), and the boundary between the two. The respective SAED patterns are shown in Figures 4c–e,. All diffraction spots in Figures 4c and d can be indexed to those of the [110] zone axes of diamondlike Si and tetragonal In, respectively. Streaking of the reflections in the underfocused electron diffraction patterns shown on the right-hand panels of Figures 4c,d implies that the preferred growth directions of the Si and In nanowires are close to the $[\bar{1}13]$ and $[1\bar{1}4]$ orientations, respectively. A HRTEM image taken from the Si domain is depicted in Figure 5a. This indicates the clearly resolved interplanar fringes (3.10 Å) that correspond to the {111} lattice distances. The inset in Figure 5a is the [110] projection of a diamondlike Si crystal lattice. Furthermore, HRTEM analysis reveals that the crystalline Si nanowire is free from planar defects and is coated with an amorphous silica sheath. The pattern taken from the boundary region between the Si and In segments shown in Figure 4e implies that the (002) plane of Si (marked with a circle) is nearly parallel to the $(1\bar{1}2)$ plane of In

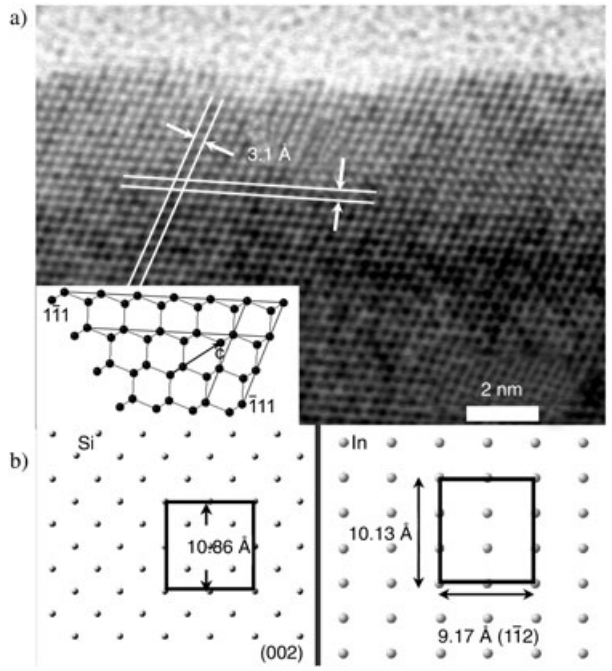

Figure 5. a) High-resolution TEM image of a Si subnanowire in which sets of {111} ($d_{111}=3.135$ Å) planes are marked with double lines; the inset shows the scheme of a diamondlike Si crystal structure viewed along the [110] direction; b) structural model showing the (002) plane of diamondlike Si and the (1$\bar{1}$2) plane of tetragonal In.

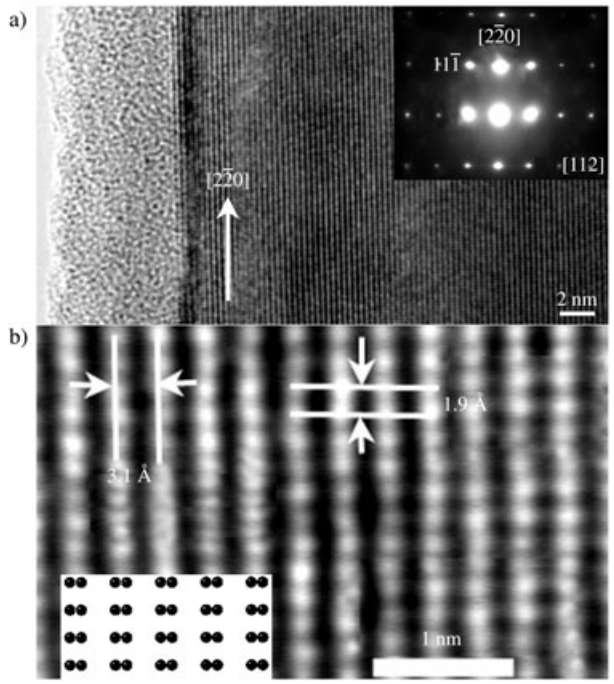

Figure 6. a) TEM image of a Si subnanowire in which the inset shows the corresponding SAED pattern; b) HRTEM image of Si subnanowire growth along the [1$\bar{1}$0] direction ($d_{11\bar{1}}=3.13$ Å, $d_{2\bar{2}0}=1.92$ Å, indicated by double lines) in which the inset shows the scheme of the diamondlike Si crystal structure viewed along the [112] direction.

(marked with a square). Figure 5b shows the structural model of diamondlike Si on the (002) plane and that of tetragonal In on the (1$\bar{1}$2) plane. The square dimensions on the Si (002) plane are close to those of the rectangle on the In (1$\bar{1}$2) plane. Thus it is reasonable to suggest that the growth of Si and In nanowires is crystallographically related.

The HRTEM image of a Si branch in Figure 6a clearly shows that a Si crystalline core is sheathed by an $\approx$8-nm thick amorphous silica shell. The spots on the corresponding SAED pattern (Figure 6a, inset) can be indexed to the [112]-zone axis of a diamondlike Si crystal. The clearly resolved interplanar fringes of 3.10 Å and 1.90 Å are observed in the HRTEM image (Figure 6b). These coincide with the (111) and (220) lattice spacings, respectively, of a diamondlike Si crystal. The HRTEM image is consistent with the projection of the diamondlike Si crystal along the [112] orientation, as shown in the inset of Figure 6b. The [2$\bar{2}$0] preferential growth orientation is also confirmed by the SAED pattern and the HRTEM image. Some other preferential growth orientations such as [1$\bar{1}$1] and [3$\bar{3}$1] are illustrated in the Supporting Information.

VLS or OA growth mechanisms are generally attributed to the anisotropic growth of Si nanowires. During the VLS-growth process,[17,18] a metal nanoparticle acts as a preferential site for vapor absorption to form a liquid alloy. Once an absorbed reactant is supersaturated within a liquid alloy at a given temperature, it nucleates from the supersaturated liquid droplet. Further condensation of the reactant vapors on the alloy droplets may result in the continuous axial growth of Si nanowires. It is crucial for VLS growth that one end of the Si nanowire is capped with an alloy droplet. Si nanowires generated by the VLS process are generally oriented along the [111] axis. In contrast, Si atom supersaturation during OA growth ranges from negligible to moderate.[19–22]

The Si nanowires presented herein are sheathed with amorphous silica along their entire lengths. The presence of oxygen leads to the formation of amorphous silica and has a significant effect on the surface stability of crystalline Si. This may promote the anisotropic growth of Si nanowires. Various growth directions have been documented for Si nanowires generated by OA growth.[21,22] Given that various orientations are possible for the anisotropic growth of Si nanowires sheathed with amorphous silica, it is assumed that their growth is determined by an OA-growth process. Silicon oxide clusters are stable in the gas phase at high temperatures.[23] They facilitate the nucleation and growth of Si nanostructures.[20] Disproportionation of SiO to Si and SiO_2 can result in the growth of Si nanowires.[19–22] During the synthesis process, SiO powder may sublime to generate a SiO vapor. At 1400 °C, the equilibrium pressure of metallic In is as high as $\approx$1000 Pa. If brought by an Ar gas flow to a lower-temperature region ($\approx$900 °C), In vapor condenses to produce liquid In droplets. Gaseous SiO deposits on the In droplets and subsequently disproportionates to generate Si nanocrystals and an amorphous silica sheath. Anisotropic growth of Si nanocrystals by the OA process results in the formation of Si nanowires sheathed with amorphous silica. At $\approx$900 °C, atomic mobility is high enough to allow self-assembly of newly arrived atoms within the growing edges and to promote the fast growth of silica nanotubes on the In droplets.[24] During the growth of Si

nanowires, silica nanotubes may grow in the opposite direction. Meanwhile, a condensed In vapor is drawn into the nanometer-sized cavity of silica nanotubes through capillarity.[25] No indium oxide is observed, as the bonding energy of Si–O (798.8 kJ mol^{-1}) is much higher than that of In–O (360.21 kJ mol^{-1}).[26] Consequently, a uniform SiO_2 sheath is formed along an entire In–Si contact. When the furnace temperature is lower than the melting point of metallic In (156.6 °C), columns of liquid In confined within silica nanotubes transform into solid In nanowires. The crystalline Si nanowires may have a certain impact on the crystallization of In nanowires, as both materials have closely related crystallographic features, as demonstrated in Figure 4. Owing to a volume decrease of an In column upon crystallization, an empty amorphous silica nanotube may remain above an In–Si heterojunction as shown in Figure 2a.

Finally, the thermal expansion of an In column confined within a silica nanotube and adjacent to a Si segment was investigated by means of a Gatan heating holder attached to the TEM. Figure 7 shows consecutive TEM images of an In column under heating. Initially the In column jumps abruptly upon melting (m.p. 156.6 °C), a consequence of the significant density difference between the solid and liquid In phases. Next the In column expands linearly with increasing temperature, in accord with the thermal-expansion behavior of bulk metallic In (or Ga).[27,28] The expansion of a liquid In column as a part of an In–Si 1D heterojunction sheathed with silica may permit the smart design of a temperature-driven switch and/or sensor within an electronic device.

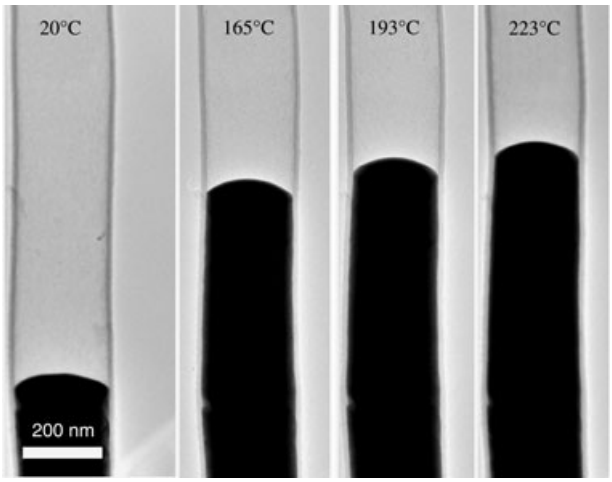

Figure 7. Consecutive TEM images of melting and thermal expansion of an In column (the part of an In–Si heterojunction) confined within a silica tube during TEM heating in situ.

In conclusion, simultaneous thermal evaporation of In and SiO powders has been shown to generate end-to-end In–Si nanowire contacts that are uniformly sheathed with amorphous silica. Within a junction, the In and Si fragments are crystallographically oriented with respect to each other. The In branch of a given junction, confined within the silica nanotube, displays a thermal expansion similar to that of bulk metallic In which opens prospects for the design of a unique temperature-driven switch and/or sensor within a metal–semiconductor electronic device.

Experimental Section

The In–Si nanowire heterojunctions were synthesized in a vertical induction furnace equipped with a fused-quartz tube and an induction-heated cylinder made of high-purity graphite coated with a carbon fiber thermoinsulating layer. The furnace was equipped with an inlet C pipe on top, and an outlet C pipe at the base. A graphite crucible that contained a ground mixture of In (1.15 g) and SiO (0.44 g) was placed in the center cylinder zone. After evacuation of the quartz tube to $\approx 10^{-3}$ Pa, a pure Ar flow was set within the carbon cylinder at a constant rate of 1000 std cm^3 min^{-1}. The furnace was heated to and kept at 1400 °C for 1 h. After the reaction was terminated and the furnace cooled to room temperature, a gray-colored product was collected from the cylinder outlet. The product was characterized by powder XRD (RINT 2200) with $Cu_{K\alpha}$ radiation ($\lambda = 1.5418$ Å), SEM (JSM-6700F), and by means of HRTEM (JEM-3000F) on a field-emission (300 kV) energy-filtered (Omega Filter) electron microscope (JEM-3100F; JEOL) equipped with an energy-dispersive X-ray spectrometer.

Received: December 5, 2004
Published online: February 23, 2005

Keywords: indium · nanostructures · nanotubes · semiconductors · silicon

[1] a) X. F. Duan, Y. Huang, R. Agarwal, C. M. Lieber, *Nature* **2003**, *421*, 241–245; b) Y. Cui, C. M. Lieber, *Science* **2001**, *291*, 851–853; c) M. Law, D. Sirbuly, J. Johnson, J. Goldberger, R. Saykally, P. Yang, *Science* **2004**, *305*, 1269–1273.

[2] a) Y. Xia, G. M. Whitesides, *Angew. Chem.* **1998**, *110*, 568–594; *Angew. Chem. Int. Ed.* **1998**, *37*, 550–575; b) Y. Xia, P. Yang, Y. Sun, Y. Wu, B. Mayers, B. Gates, Y. Yin, F. Kim, Y. Yan, *Adv. Mater.* **2003**, *15*, 353–389; c) D. Wang, H. Dai, *Angew. Chem.* **2002**, *114*, 4977–4980; *Angew. Chem. Int. Ed.* **2002**, *41*, 4783–4786; d) J. Zhan, X. Yang, D. Wang, S. Li, Y. Xia, Y. Qian, *Adv. Mater.* **2000**, *12*, 1348–1351; e) G. R. Patzke, F. Krumeich, R. Nesper, *Angew. Chem.* **2002**, *114*, 2554–2571; *Angew. Chem. Int. Ed.* **2002**, *41*, 2446–2461; f) C. N. R. Rao, F. L. Deepak, G. Gundiah, A. Govindaraj, *Prog. Solid State Chem.* **2003**, *31*, 5–147; g) R. Q. Zhang, Y. Lifshitz, S. T. Lee, *Adv. Mater.* **2003**, *15*, 635–640; h) B. Liu, S. Yu, L. Li, Q. Zhang, F. Zhang, K. Jiang, *Angew. Chem.* **2004**, *116*, 4849–4854; *Angew. Chem. Int. Ed.* **2004**, *43*, 4745–4750; i) J. Liu, Q. Li, T. Wang, D. Yu, Y. Li, *Angew. Chem.* **2004**, *116*, 5158–5162; *Angew. Chem. Int. Ed.* **2004**, *43*, 5048–5052; j) A. R. Armstrong, G. Armstrong, J. Canales, P. G. Bruce, *Angew. Chem.* **2004**, *116*, 2336–2338; *Angew. Chem. Int. Ed.* **2004**, *43*, 2286–2288.

[3] S. M. Sze, *Physics of Semiconductor Devices*, Wiley, New York, **1981**.

[4] M. S. Gudiksen, L. J. Lauhon, J. Wang, D. C. Smith, C. M. Lieber, *Nature* **2002**, *415*, 617–620.

[5] Y. Wu, R. Fan, P. Yang, *Nano Lett.* **2002**, *2*, 83–86.

[6] M. T. Bjork, B. J. Ohlsson, T. Sass, A. I. Persson, C. Thelander, M. H. Magnusson, K. Deppert, L. R. Wallenberg, L. Samuelson, *Nano Lett.* **2002**, *2*, 87–89.

[7] L. J. Lauhon, M. S. Gudiksen, D. Wang, C. M. Lieber, *Nature* **2002**, *420*, 57–61.

[8] J. Hu, M. Ouyang, P. Yang, C. M. Lieber, *Nature* **1999**, *399*, 48–51.

[9] Y. Wu, J. Xiang, C. Yang, W. Lu, C. M. Lieber, *Nature* **2004**, *430*, 61 – 65.
[10] *Future Trends in Microelectronics: The Road Ahead* (Eds: S. Luryi, J. M. Xu, A. Zaslavsky), Wiley, New York, **1999**.
[11] a) A. Liu, R. Jones, L. Liao, D. Samara-Rubio, D. Rubin, O. Cohen, R. Nicolaescu, M. Paniccia, *Nature* **2004**, *427*, 615 – 618; b) N. Mathur, *Nature* **2002**, *419*, 573 – 575.
[12] a) Y. Wu, Y. Cui, L. Huynh, C. J. Barrelet, D. C. Bell, C. M. Lieber, *Nano Lett.* **2004**, *4*, 433 – 436; b) J. D. Holmes, K. P. Johnston, R. C. Doty, B. Korgel, *Science* **2000**, *287*, 1471 – 1473; c) S. T. Lee, Y. F. Zhang, N. Wang, Y. H. Tang, I. Bello, C. S. Lee, *J. Mater. Res.* **1999**, *14*, 4503 – 4507; d) G. Gundiah, F. L. Deepak, A. Govindaraj, C. N. R. Rao, *Chem. Phys. Lett.* **2003**, *381*, 579 – 583.
[13] K. Soulantica, A. Maisonnat, F. Senocq, M. C. Fromen, M. J. Casanove, B. Chaudret, *Angew. Chem.* **2001**, *113*, 3071 – 3074; *Angew. Chem. Int. Ed.* **2001**, *40*, 2984 – 2986.
[14] Y. Li, X. Li, Z. Deng, B. Zhou, S. Fan, J. Wang, X. Sun, *Angew. Chem.* **2002**, *114*, 343 – 345; *Angew. Chem. Int. Ed.* **2002**, *41*, 333 – 335.
[15] A. Rogachev, A. Bezryadin, *Appl. Phys. Lett.* **2003**, *83*, 512 – 514.
[16] P. Schwerdtfeger, *Angew. Chem.* **2003**, *115*, 1936 – 1939; *Angew. Chem. Int. Ed.* **2003**, *42*, 1892 – 1895.
[17] A. M. Morales, C. M. Lieber, *Science* **1998**, *279*, 208 – 211.
[18] Y. Wu, P. Yang, *J. Am. Chem. Soc.* **2001**, *123*, 3165 – 3166.
[19] D. D. D. Ma, C. S. Lee, F. C. K. Au, S. Y. Tong, S. T. Lee, *Science* **2003**, *299*, 1874 – 1877.
[20] R. Q. Zhang, M. W. Zhao, S. T. Lee, *Phys. Rev. Lett.* **2004**, *93*, 095503-1–095503-4.
[21] T. Y. Tan, S. T. Lee, U. Gösele, *Appl. Phys. A* **2002**, *74*, 423 – 432.
[22] C. P. Li, C. S. Lee, X. L. Ma, N. Wang, R. Q. Zhang, S. T. Lee, *Adv. Mater.* **2003**, *15*, 607 – 609.
[23] L. Brewer, *Chem. Rev.* **1953**, *53*, 1 – 75.
[24] Z. R. Dai, Z. W. Pan, Z. L. Wang, *Adv. Funct. Mater.* **2003**, *13*, 9 – 24.
[25] P. M. Ajayan, S. Iijima, *Nature* **1993**, *361*, 333 – 334.
[26] *Lange's Handbook of Chemistry*, 15th ed. (Ed.: J. A. Dean), McGraw-Hill, New York, **1999**, section 4.
[27] Y. Li, Y. Bando, D. Golberg, *Adv. Mater.* **2004**, *16*, 37 – 40.
[28] Y. Gao, Y. Bando, *Nature* **2002**, *415*, 599 – 599.

